HOKKAIDO UNIVERSITY

Title	Global search for low-lying crystal structures using the artificial force induced reaction method : A case study on carbon
Author(s)	Takagi, Makito; Taketsugu, Tetsuya; Kino, Hiori et al.
Citation	Physical Review B, 95(18), 184110 https://doi.org/10.1103/PhysRevB.95.184110
Issue Date	2017-05-30
Doc URL	https://hdl.handle.net/2115/67066
Rights	©2017 American Physical Society
Type	journal article
File Information	PhysRevB95 184110.pdf

Hokkaido University Collection of Scholarly and Academic Papers : HUSCAP

Global search for low-lying crystal structures using the artificial force induced reaction method: A case study on carbon

Makito Takagi,[1] Tetsuya Taketsugu,[2] Hiori Kino,[3,4] Yoshitaka Tateyama,[3] Kiyoyuki Terakura,[3] and Satoshi Maeda[2,*]

[1]*Graduate School of Chemical Sciences and Engineering, Hokkaido University, Kita 13, Nishi 8, Kita-ku, Sapporo 060-8628, Japan*

[2]*Department of Chemistry, Faculty of Science, Hokkaido University, Kita 10, Nishi 8, Kita-ku, Sapporo 060-0810, Japan*

[3]*Center for Materials Research by Information Integration, National Institute for Materials Science, 1-2-1, Sengen, Tsukuba 305-0047, Japan*

[4]*ESICMM, National Institute for Materials Science, Tsukuba, 1-2-1, Sengen, Ibaraki 305-0047, Japan*

(Received 16 February 2017; revised manuscript received 29 March 2017; published 30 May 2017)

We propose an approach to perform the global search for low-lying crystal structures from first principles, by combining the artificial force induced reaction (AFIR) method and the periodic boundary conditions (PBCs). The AFIR method has been applied extensively to molecular systems to elucidate the mechanism of chemical reactions such as homogeneous catalysis. The present PBC/AFIR approach found 274 local minima for carbon crystals in the C_8 unit cell described by the generalized gradient approximation–Perdew-Burke-Ernzerhof functional. Among many newly predicted structures, three low-lying structures, which exhibit somewhat higher energy compared with those previously predicted, such as Cco-C_8 (Z-carbon) and M-carbon, are further discussed with calculations of phonon and band dispersion curves. Furthermore, approaches to systematically explore two- or one-dimensional periodic structures are proposed and applied to the C_8 unit cell with the slab model. These results suggest that the present approach is highly promising for predicting crystal structures.

DOI: 10.1103/PhysRevB.95.184110

I. INTRODUCTION

Properties of materials depend not only on their composition but also on their crystal structure. Different crystal structures are formed depending on the generation conditions. For example, carbon can take various forms [1], such as diamond, graphite, lonsdaleite (hexagonal diamond), fullerene, carbon nanotube (CNT), graphene, graphene nanoribbon (GNR), and so on. Furthermore, many stable structures have been predicted theoretically. M-carbon [2,3], Cco-C_8 or Z-carbon [4,5], and so forth have been predicted recently from first principles. As many as 315 different structures have already been registered to the Samara carbon allotrope database (SACADA) [6], and there has been a debate regarding how to handle newly predicted structures [7]. All the 460 reference papers we gathered as those regarding known carbon crystal structures are cited in S1 in Supplemental Material [8]. Two- or one-dimensional periodic structures, such as graphene and CNT, have also attracted attention as novel materials and catalysts.

In this context, the crystal structure prediction from first principles has become one of the active fields in materials science. To date, various methods have been developed [9–12]. Methods for the searching of two-dimensional periodic structures have also been proposed [13]. In one sense, the crystal structure prediction is to find the most stable structure of a given atomic composition. Finding only the most stable structure would be easy in a small system such as C_8 in which the number of atoms in the unit cell is only eight. Development of methods that can find the lowest-energy structure in more complex systems therefore is an important research direction. On the other hand, there would be another direction, that is, to exhaustively enumerate possible low-lying structures of a given atomic composition. This still is not a trivial task even in a small system such as the C_8 unit cell which is the focus of the present study.

In this paper, we combined the artificial force induced reaction (AFIR) [14–16] method with the periodic boundary conditions (PBCs). The AFIR method has previously been employed extensively in automated exploration of structures and reaction pathways in molecular systems such as homogeneous catalysis [17]. The present extension enables the exhaustive search for low-lying crystal structures by the AFIR method. As a case study, crystal structures of carbon described by the C_8 unit cell were explored by the PBC version of the AFIR method. The search generated 274 local minimum (MIN) crystal structures starting from a single initial structure. The obtained extensive structural database includes not only known structures but also many unreported structures. Additional implementations for the exploration of two- or one-dimensional periodic structures with the slab model were also introduced and applied to carbon in the C_8 unit cell. The search yielded 122 and 49 local minimum structures for the two- and one-dimensional periodic systems, respectively. These results demonstrate the usefulness of the present approach in a systematic exploration of unknown crystal structures from first principles.

II. METHOD

A. AFIR method

The AFIR method pushes fragments A and B together or pulls them apart to induce a structural rearrangement. In Fig. 1, a schematic of the AFIR method is shown. The product can be easily reached simply by minimizing a model function, termed the AFIR function (dotted curve), which is composed of the potential energy surface (PES) and the force term (for the form of the force term, see Ref. [14]). As demonstrated previously [14–16], the minimization path of this function, termed the AFIR path, is a good approximation of the reaction path of the corresponding structural rearrangement. Although the first-order saddle point along the path can also be determined

*smaeda@eis.hokudai.ac.jp

 ©2017 American Physical Society

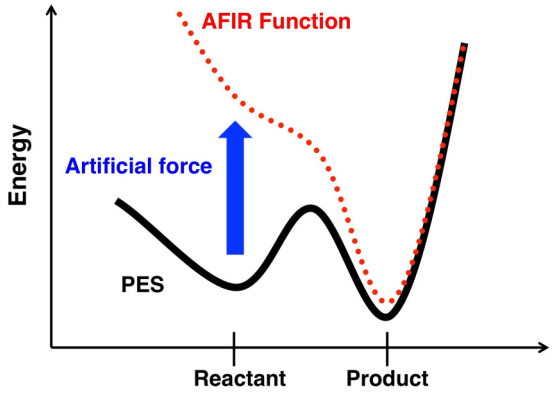

FIG. 1. A schematic of the AFIR method. Starting from the reactant region, the product region can be easily found by minimizing the AFIR function (dotted curve), which is composed of the PES and the force term (for the form of the force term, see Ref. [14]). By repeating the minimization of the AFIR function with systematically generated different force terms, it is possible to obtain many different products starting from a given initial structure.

by geometry optimization starting from the highest-energy point along the AFIR path, the saddle-point optimization was not performed in this study because the present purpose was to explore MIN structures. In this study, the model collision energy parameter γ, which defines the strength of the artificial force [14], was set to a sufficiently large value, i.e., 1000.0 kJ/mol, so as not to limit the search area.

There are two modes in the AFIR method, i.e., the multicomponent mode (MC-AFIR) and the single-component mode (SC-AFIR). The MC-AFIR was not described in this paper because it has been employed in the exploration of pathways of bimolecular or multicomponent reactions [14,16]. In the SC-AFIR, fragments A and B were systematically defined in a given structure. The AFIR path was then computed for all the automatically defined fragment pairs. The systematic procedure to generate fragment pairs has been described in our previous reports [15,16]. The force term with a given γ is uniquely determined at any structure when the fragment pair is defined. By computing AFIR paths for different fragment pairs, various pathways that depart from the initial structure and lead to more MINs can be obtained. Further applications of the same procedure to newly obtained MINs produce many more structures.

By applying the SC-AFIR to all obtained MINs, a full network of reaction pathways in the PES area accessible by a given γ can be generated. Though such an exhaustive search can be highly demanding, some limiting search options are also available. Two such options have mainly been employed previously: a stochastic search targeted to low-energy structures and a restricted search targeted to structures having a specified chemical bond connectivity. The stochastic search option was adopted in this study to efficiently search for low-lying crystal structures, where the model temperature parameter T_R [16], which determines how frequently high-energy MINs are chosen, was set to a very large value of 10 000.0 K to explore a wide variety of structures. In the stochastic search, the calculation was terminated if the last P AFIR paths did not update the set of lowest-M MINs. In this study, M and P were set to f and $3f$, respectively, where f is the number of internal degrees of freedom defined below.

B. Internal degrees of freedom

The PBCs are used to describe periodic systems. In the search of three-dimensional crystal structures, Cartesian coordinates of three translation vectors (TVs) and all N atoms in the unit cell, i.e., $3N + 9$ Cartesian coordinates, were considered as variables. In each optimization step, a set of $3N + 3$ orthonormal vectors was defined, by eliminating three modes for the translational motions of all atoms along the x, y, and z axes and three modes for the rotational motions of the whole system around the x, y, and z axes from the $3N + 9$ Cartesian coordinates. Then, geometrical displacements were invoked in the $3N + 3$ dimensional hyperspace, since neither the three translational motions of all atoms nor the three rotational motions of the whole system changed the total energy of a system without any external field.

In the case where two-dimensional periodic structures were searched, one TV was fixed on the z axis and the other two TVs were restricted on the xy plane. In other words, the x and y coordinates of the two TVs and all N atoms in the unit cell, i.e., $3N + 4$ Cartesian coordinates, were considered as variables. In this study, the length of the TV fixed on the z axis was set to 20.0 Å. In each optimization step, a set of $3N$ orthonormal vectors was defined, by eliminating three modes for the translational motions of all atoms along the x, y, and z axes and one mode for a rotational motion of the whole system around the z axis from the $3N + 4$ Cartesian coordinates. Then, geometrical displacements were invoked in the $3N$-dimensional hyperspace.

In the case where one-dimensional periodic structures were searched, two TVs were fixed on the z and y axes, respectively, and the remaining TV was restricted on the x axis. Hence, the x coordinate of one TV and all N atoms in the unit cell, i.e., $3N + 1$ Cartesian coordinates, were considered as variables. In this study, the lengths of the two TVs fixed on the y and z axes were both set to 20.0 Å. In each optimization step, a set of $3N-3$ orthonormal vectors was defined, by eliminating three modes for the translational motions of all atoms along the x, y, and z axes and one mode for a rotational motion of the whole system around the x axis from the $3N + 1$ Cartesian coordinates. Then, geometrical displacements were invoked in the $3N-3$ dimensional hyperspace.

Many electronic structure calculation programs provide the force acting on atoms in the unit cell and the stress tensor acting on the unit cell. To perform the search in the above-mentioned coordinate system, the first derivative of the total energy for TVs, i.e., $\partial E/\partial h$, is required. In this study, $\partial E/\partial h$ was obtained with the following equation:

$$\left.\frac{\partial E}{\partial \mathbf{h}}\right|_{\mathbf{h}_0} = -V_0 \boldsymbol{\sigma}^t \mathbf{h}_0^{-1}, \tag{1}$$

where E is the potential energy, $\mathbf{h}$ is the unit cell, $\mathbf{h}_0$ is the unit cell with which the stress is calculated, V_0 is the volume of the unit cell, and $\boldsymbol{\sigma}$ is the stress tensor. The derivation of Eq. (1) is shown in S2 in Supplemental Material [8].

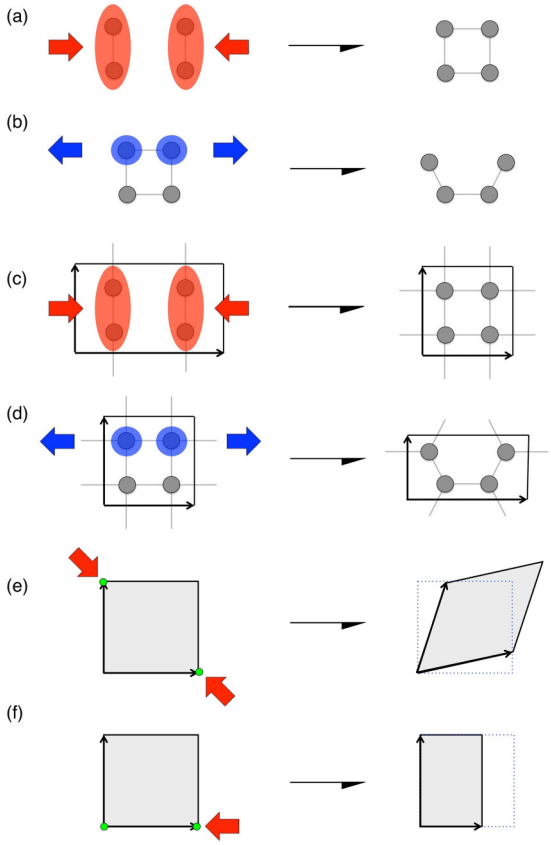

FIG. 2. Schematic of the SC-AFIR method: (a) a positive force applied to a molecular system, (b) a negative force applied to a molecular system, (c) a positive force applied to atoms in a periodic system, (d) a negative force applied to atoms in a periodic system, (e) a positive force applied to a pair of TVs, and (f) a positive force applied to the origin and one of the TVs. A green circle indicates a dummy atom.

C. SC-AFIR method with PBCs

In the conventional SC-AFIR, fragments A and B that are composed of several atoms in a given molecular system are pushed together or pulled apart by minimizing the AFIR function, as illustrated in Figs. 2(a) and 2(b). In the present implementation, a similar procedure was applied to the atoms in the unit cell, where atoms in fragments A and B were pushed together or pulled apart as depicted in Figs. 2(c) and 2(d), respectively. The algorithm to define fragments automatically was exactly the same as that proposed previously for molecular systems [15,16]. In addition, assuming that there were dummy atoms at the origin and also at the positions of TVs, a pair of dummy atoms were also pushed together or pulled apart as illustrated in Figs. 2(e) and 2(f), to consider the deformation of the unit cell.

D. Structural clustering

A crystal structure can be expressed in a number of different ways regarding the shape of the unit cell and atomic arrangements in the unit cell. For example, there were a number of ways to describe the crystal structure of graphite. With the C_8 unit cell, graphite can be written with a nearly cubic unit cell, a largely elongated cuboid unit cell, a highly distorted rhombohedral unit cell, and many others. These graphite structures have similar but slightly different energies owing to numerical errors in the first-principles calculations. Without the clustering mentioned bellow, the SC-AFIR search, which was targeted to low-energy structures, tended to be applied only to graphite (or lowest-lying structures in a given system). This is because the probability that the lowest-lying structures are selected is typically large in the stochastic algorithm [16], and in most cases, the SC-AFIR is applied to one of the lowest-lying structures expressed with different unit cells.

To overcome this problem, structural clustering was performed during the automated search. A similarity between two structures was checked by comparing them with a supercell, and those judged to be similar were regarded as belonging to the same group. From each group, the following structures were selected as representatives.

(i) The most stable structure.

(ii) The structure which has the largest χ, where χ is a quantity defined as the length of the shortest TV divided by the longest TV.

(iii) The structure which has the smallest φ, where φ is the sum of the absolute values of the inner products between all pairs of normalized TVs.

(iv) The structure which has the smallest λ, where $\lambda = (1 - \chi + \varphi)/2$.

The other structures were then excluded from the search. Structures that had a highly distorted unit cell, in which an angle between a pair of TVs was smaller than $\pi/4$ or larger than $3\pi/4$, were also excluded from the search.

Some structures that can be described only with highly elongated or largely distorted unit cells may be missed, because the above conditions avoid searches starting from structures having such unit cells. Actually, one previously reported structure, which is written with a highly elongated unit cell, was missed in the present automated search, as discussed in Sec. IV. This is a serious problem when only a small unit cell is applicable. However, even those with an elongated and/or distorted unit cell in a given cell size can be obtained with nearly cubic unit cells with a larger cell size. Any periodic structure can be described by a nearly cubic unit cell, when a sufficiently large unit cell is applied.

E. Flow of the SC-AFIR search

The search generates a set of MINs. The list of MINs obtained by the search is termed as the MIN list. The search proceeds as follows:

(1) Start from initial structure(s).

(2) Choose a pair of fragments in one of the MINs in the MIN list by the procedure described in Sec II A combined with the structural clustering introduced in Sec. II D.

(3) Minimize the AFIR function for the chosen fragment pair to obtain the AFIR path, which is the approximate reaction path.

(4) Optimize the MINs starting from local minima along the AFIR path, and add newly obtained MINs to the MIN list.

(5) Exit from the automated search if the latest P AFIR paths did not update the set of lowest-M MINs.

(6) Return to step 2, and continue the search.

The initial structure can either be one or more of the optimized MIN(s), or one or more random structure(s). In the case where the optimized MINs are given, these MINs are added to the MIN list directly. Otherwise, randomly generated initial structures are optimized, and then these optimized MINs are added to the MIN list.

In step 4, the MINs are optimized on the PES. Therefore, MINs in the MIN list are all local minima on the PES. Minimization of both the PES in step 4 and the AFIR function in step 3 are done by the rational function optimization (RFO) method [18], where the RFO step is determined for the $3N + 3$, $3N$, or $3N - 3$ internal degrees of freedom in three-, two-, or one-dimensional periodic systems, respectively, as discussed in Sec. II B. In addition, steps 2–6 can be done in parallel.

After completion of the SC-AFIR calculation, not only the most stable structure but also a huge database of low-lying structures is generated. Furthermore, their network via the AFIR path is also obtained without any additional calculation. First-order saddle points can be located by optimizing the AFIR path by any path-optimization method. It is also possible to obtain the reaction path network via the steepest descent path (SDP) starting from the first-order saddle points, by the additional SDP calculations. Systematic study on the path network in the crystal system generated by the SC-AFIR method will be the subject of future work.

F. Electronic structure calculation

SIESTA3.2 [19–21] was used to compute the energy, force acting on atoms, and stress tensor acting on a unit cell. These calculations were performed using density functional theory (DFT) with the Perdew-Burke-Ernzerhof (PBE) functional and the DZP basis set. Grimme's dispersion correction [22], with the parameters $R_0 = 2.904$ Å and $C6 = 4.0\,\mathrm{kJ\,Å^6\,mol^{-1}}$, was added, where the value of $C6$ was adjusted so that the present computation reproduced the interlayer distance of graphite of 3.4 Å. The pseudopotential of carbon was prepared using the parameters in the GGA Pseudopotential Database [23], where the core correction was not considered. A Monkhorst-Pack grid was, respectively, set to $4 \times 4 \times 4$,$4 \times 4 \times 1$, or $4 \times 1 \times 1$, including the Γ point in the searches for three-, two-, or one-dimensional periodic structures for the k-point sampling. Collinear spin alignment was taken into account. The electronic temperature was set to 5.0 K. The mesh cutoff value was set to 50.0 Ry in the automated search, and finally increased to 200.0 Ry; all structures discussed below are optimized MINs on the PES with the higher mesh cutoff value.

G. Computational procedure

The concrete procedure in this study of searching for low-lying crystal structures of the carbon systems proceeds along the following five steps:

(a) Generate an initial structure in the C_4 unit cell by optimizing a random structure.

(b) Search for MINs with the C_4 unit cell by the SC-AFIR starting from the single initial structure generated in step (a).

(c) Generate initial structures in the C_8 unit cell by extending the unit cell in MINs obtained for the C_4 unit cell in step (b) along the shortest TV of each MIN, and then reoptimizing them in the C_8 unit cell.

TABLE I. Degrees of freedom f, the number of obtained AFIR paths N_{path}, obtained MIN structures N_{MIN}, and gradient calculations required in each step N_{gradient}, in the search of three-dimensional structures of carbon. A single gradient calculation includes calculations of the energy, force, and stress tensor.

Step[a]	f	N_{path}	N_{MIN}	N_{gradient}
(a)	15		1	34
(b)	15	158	35	46838
(c)	27		24	2010
(d)	27	697	377	323321
(e)	27		274	19653

[a]Steps (a)–(e) are described in Sec. II G.

(d) Search for MINs with the C_8 unit cell by the SC-AFIR starting from the initial structures obtained in step (c).

(e) Reoptimize all structures generated in step (d) in the C_8 unit cell with the higher mesh cutoff value (200.0 Ry).

Finally, further analyses were conducted for the important crystal structures obtained. Spglib-1.8.3 was used to determine the space group of the obtained crystal structures [24]. Phonopy-1.10.8 was used to calculate the phonon dispersion [25,26]. Prior to the band and phonon calculations, the corresponding structure was reoptimized with a Monkhorst-Pack grid of $12 \times 12 \times 12$ and was shown in the Supplemental Material [8]. The band dispersion was calculated with gnubans in SIESTA3.2. The k paths were determined according to the method previously described in the literature [27].

III. RESULTS

A. Three-dimensional crystal structures of carbon with the C_8 unit cell

The search was initiated from a single MIN obtained by optimizing a randomly generated structure in the C_4 unit cell, where the initial random structure is shown in S3 in Supplemental Material [8]. In total, 274 MINs were obtained after the five steps (a)–(e) described in Sec. II G. Table I shows degrees of freedom in each system, the numbers of AFIR paths and MINs obtained after each step, and the number of gradient calculations required to finish each step. Cartesian coordinates of all the 274 MINs are shown in S4 in Supplemental Material [8].

The 30 most stable MINs among the 274 MINs are shown in Fig. 3, where the Nth -lowest MIN is labeled as 3D-min N. The names of those known previously, either experimentally or theoretically, are also shown in the structural labels. The space groups indicated in the structural labels were determined by spglib-1.8.3. The energy values are relative to the most stable structure, hexagonal graphite (3D-min0). Both of the known graphite structures, hexagonal (alpha) and rhombohedral (beta), were obtained as 3D-min0 and 3D-min2, respectively. The former, with AB stacking, showed a lower energy than the latter having ABC stacking, consistent with the previously acquired knowledge. Hexagonal graphite (3D-min0) showed a lower energy than cubic diamond (3D-min1), and this was also consistent with the known trend. The structure with AA stacking was not a local minimum with the present setup for electronic structure calculation, where the

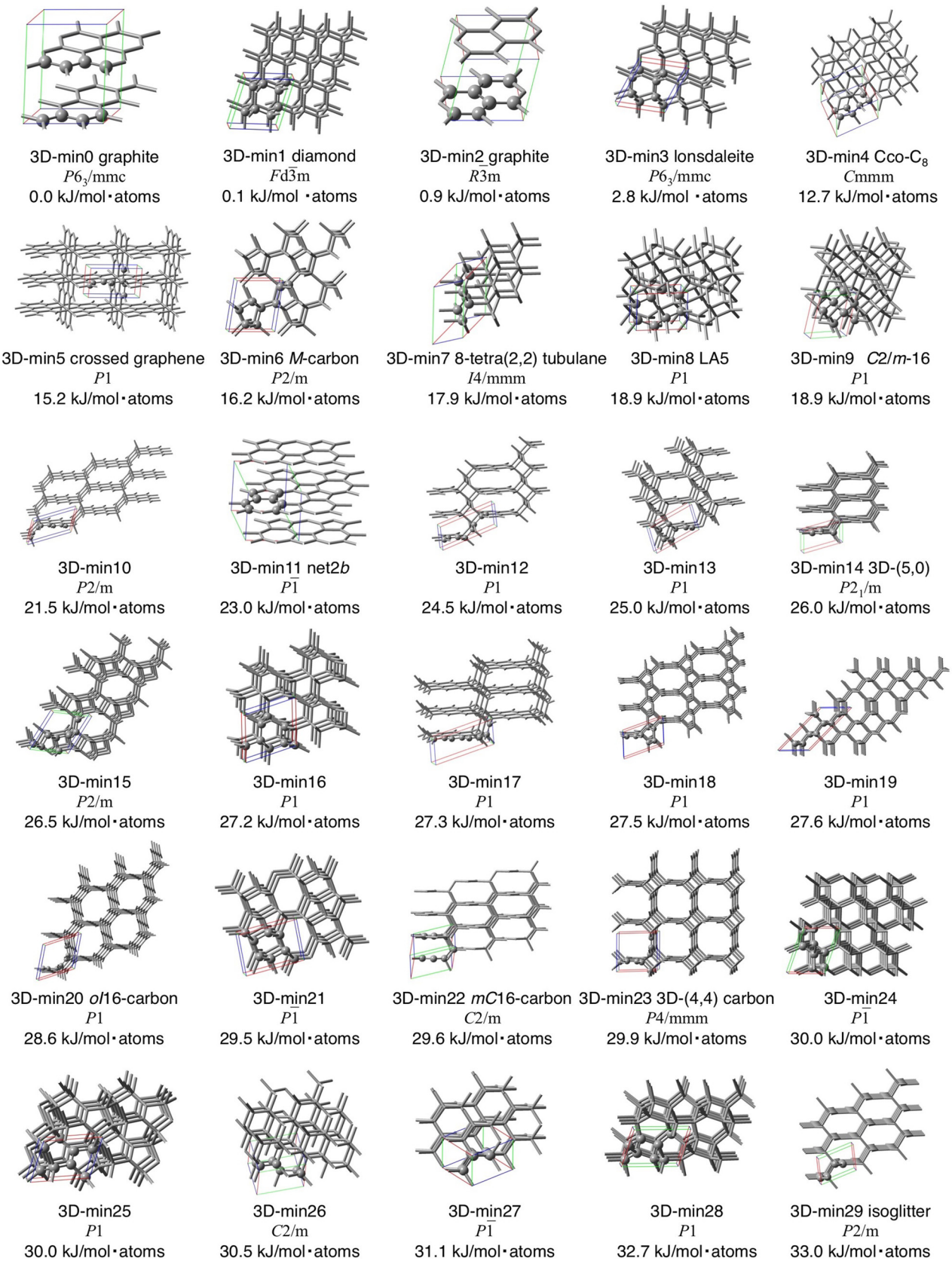

FIG. 3. Thirty of the most stable crystal structures of carbon with the C_8 unit cell. The names of structures (if available), space groups, and relative energies are shown in the labels. TVs are shown as red, green, and blue lines. Atoms in a unit cell are highlighted by the ball model.

geometry optimization starting from such an initial structure collapsed into hexagonal graphite. Note that cubic diamond was energetically more stable than hexagonal graphite when the original PBE-D2 parameters were used together with the present setup for electronic structure calculation. This would arise from the parameters such as the DZP basis set, or the parameters such as the pseudopotential, charge density cutoff, and k mesh and so forth that were adopted in this study. In this study, by adjusting the $C6$ value of the PBE-D2 parameters, the energetics in Fig. 3, which was consistent with the previously acquired knowledge, was obtained. We also notice that the energy difference between hexagonal graphite and cubic diamond in Fig. 3 is still smaller than that in the more elaborate calculation (∼3 kJ/mol atoms) [28].

Many previously reported structures, such as hexagonal graphite (3D-min0), cubic diamond (3D-min1), rhombohedral graphite (3D-min2), lonsdaleite (or hexagonal diamond) (3D-min3), Cco-C_8 or Z-carbon (3D-min4) [4,5], crossed graphene (3D-min5) [29], M-carbon (3D-min6) [2,3], 8-tetra(2,2) tubulane or bct C_4 (3D-min7) [30–39], LA5 or Y carbon (3D-min8) [38,40], $C2/m$-16 (3D-min9) [41], 3D-(5,0) (3D-min14) [39], oI16-carbon (3D-min20) [42], mC16-carbon (3D-min22) [42], 3D-(4,4) carbon or squaroglitter (3D-min23) [39,43], isoglitter (3D-min29) [44], 8-tetra(3,3) tubulane or E (3D-min33) [30,36,38,45], LA7 (3D-min52) [38], diam_cr43_bo (3D-min57) [46], LA10 (3D-min69) [47], a hypothetical metallic allotrope of carbon or bct-4 carbon (3D-min82) [2,48–51], and F (3D-min196) [36], were found in the automated search. The correspondence between the previously reported structures and those obtained by the present search was determined by comparing our structures with those with 2, 4, 8, and 16 atoms per unit cell in the SACADA [6], except for the case of 3D-min5 and 3D-min11. 3D-min11 is a structure in which net2b [52], a two-dimensional sheet composed of five- and seven-membered rings, is stacked.

In Fig. 3, 8-tetra(3,3) tubulane (3D-min33), LA7(3D-min52), diam_cr43_bo (3D-min57), LA10 (3D-min69), hypothetical metallic allotrope of carbon (3D-min82), and F (3D-min196) are not shown because these structures have higher energies of 35.2, 39.7, 41.1, 46.1, 50.1, and 80.2 kJ/mol atoms, respectively. To the best of our knowledge, the other structures have not previously been reported. This demonstrates that the present approach is useful for exploring unknown crystal structures.

B. Two-dimensional periodic structures of carbon with the C_8 unit cell

The search for the two-dimensional structures was also initiated from a single MIN obtained by optimizing a randomly generated structure in the C_4 unit cell, where the initial random structure is shown in S3 in Supplemental Material [8]. In total, 122 MINs were obtained after the five steps (a)–(e) described in Sec. II G. Table II shows degrees of freedom in each system, the numbers of AFIR paths and MINs obtained after each step, and the numbers of gradient calculations required to finish each step. Cartesian coordinates of all the 122 MINs are shown in S4 in Supplemental Material [8].

The low-lying 15 structures are shown in Fig. 4. The Nth -lowest structure is labeled as 2D-min N. The names of those known previously, either experimentally or theoretically, are shown in the structural labels. The energy values are relative to the most stable structure, hexagonal graphite (3D-min0).

TABLE II. Degrees of freedom f, the number of obtained AFIR paths N_{path}, obtained MIN structures N_{MIN}, and gradient calculations required in each step N_{gradient}, in the search of two-dimensional structures of carbon. A single gradient calculation includes calculations of the energy, force, and stress tensor.

Step[a]	f	N_{path}	N_{MIN}	N_{gradient}
(a)	12		1	42
(b)	12	87	28	16623
(c)	24		24	1524
(d)	24	572	237	153965
(e)	24		122	14082

[a]Steps (a)–(e) are described in Sec. II G.

The lowest-lying structure is the four-layer graphite (2D-min0-2). A graphene sheet can be written with a unit cell including two carbon atoms. With eight carbon atoms, not only graphene but also four-layer and bilayer graphite can be obtained. The stacking type of 2D-min0 is ABCA. In 2D-min1, the bottom three layers adopt an ABC stacking. The top layer is similar to, but slightly deviated from B. In 2D-min2, the bottom three layers show an ABB stacking, although the top layer is deviated from all the other three. The slight deviation from the ABC layers seen in 2D-min1 and 2D-min2 arises from the present setup of the electronic structure calculation, which is not very accurate for describing weak interactions. Bilayer graphite (2D-min3) with an AB stacking and graphene (2D-min4) are the next most stable structures. In addition, a lot of sheet structures that contain three-, four-, five-, six-, seven-, eight-, nine-, and/or ten-membered rings were obtained, where some of them correspond to those predicted from graph theory, such as net 2b (2D-min5) [52–55], pentahexoctite (2D-min6) [56], and network7 (2D-min23) [53,57–61]. Carbynes are stabilized by interacting with a graphene (2D-min7-12, 2D-min14-18). Although they all are clusters between graphene and carbyne, they are different to each other in their interaction sites. In addition, two-dimensional sheets with a certain thickness, such as layered diamond [62] (2D-min19) and related structures (2D-min20-22), were also found.

C. One-dimensional periodic structures of carbon with the C_8 unit cell

The search for one-dimensional structures was initiated from a single MIN obtained by optimizing a randomly generated structure in the C_4 unit cell, where the initial random structure is shown in S3 in Supplemental Material [8]. In total, 49 MINs were obtained after the five steps (a)–(e) described in Sec. II G. Table III shows degrees of freedom in each system, the numbers of AFIR paths and MINs obtained after each step, and the numbers of gradient calculations required to finish each step. Cartesian coordinates of all the 49 MINs are shown in S4 in Supplemental Material [8].

The low-lying 15 structures are shown in Fig. 5. The Nth-lowest structure is labeled as 1D-min N. The names of the structures known previously, either experimentally or theoretically, are shown in the structural labels. The energy

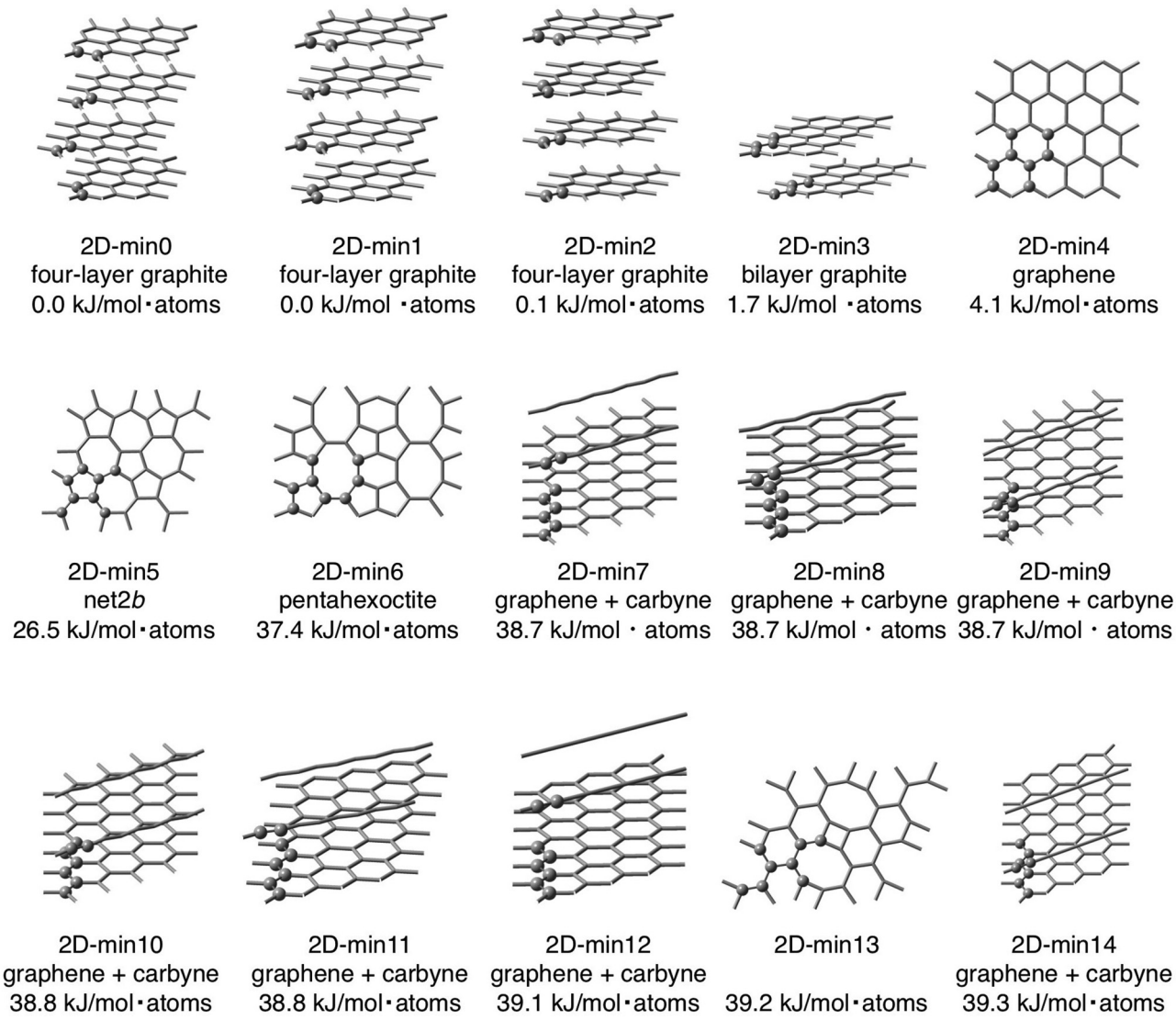

FIG. 4. Fifteen low-lying two-dimensional periodic structures of carbon with the C_8 unit cell. The names of the structures (if available) and relative energies are shown in the labels. Atoms in a unit cell are highlighted by the ball model.

values are relative to the most stable structure, hexagonal graphite (3D-min0).

The most stable structure is GNR (1D-min0). Another stable structure is the (2,2)-CNT (1D-min1, 1D-min2), which is the smallest CNT. 1D-min2 is elongated along the x axis compared with 1D-min1. 1D-min3–1D-min5 are clusters of GNR and carbyne that resemble each other. These three are different in their interaction sites. Carbyne (1D-min9, 1D-min13, 1D-min14,) is less stable than the GNR-carbyne clusters (1D-min3–1D-min5). The polyacenelike thinnest GNR (1D-min25) was found as the 26th most stable structure. Some structures containing three-, four-, five-, six-, seven-, eight-, nine-, and/or ten-membered rings were also found as higher-energy structures.

TABLE III. Degrees of freedom f, the number of obtained AFIR paths N_{path}, obtained MIN structures N_{MIN}, and gradient calculations required in each step N_{gradient}, in the search of one-dimensional structures of carbon. A single gradient calculation includes calculations of the energy, force, and stress tensor.

Step[a]	f	N_{path}	N_{MIN}	N_{gradient}
(a)	9		1	16
(b)	9	114	63	13499
(c)	21		42	2992
(d)	21	447	201	66230
(e)	21		49	10901

[a]Steps (a)–(e) are described in Sec. II G.

IV. DISCUSSION

Among the newly found crystal structures, 3D-min10 is the most stable. Its structure is shown in various ways in Fig. 6. Its primitive lattice contains eight carbon atoms, and its space group is $P2/m$. This structure is composed of sp^2 and sp^3 carbons and corresponds to a structure in which graphene sheets in graphite are connected to each other by C-C bonds. We note that a similar structure has previously been reported as diam_cr43_bo (3D-min57) [46]. The difference is whether

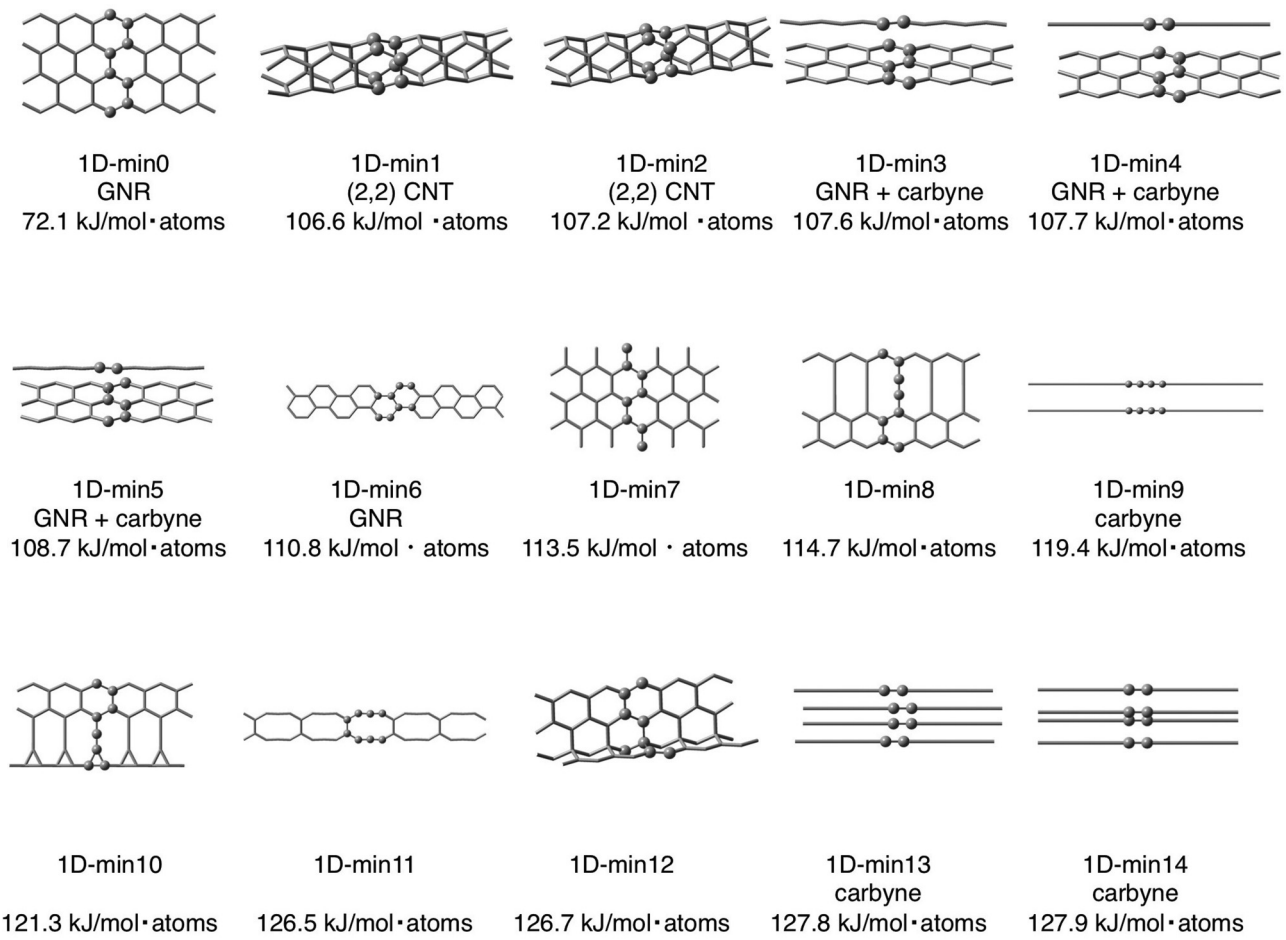

FIG. 5. Fifteen low-lying one-dimensional periodic structures of carbon with the C_8 unit cell. Names of structures (if available) and relative energies are shown in labels. Atoms in a unit cell are highlighted by the ball model.

or not the structures contain four-membered rings; 3D-min10 does not have a four-membered ring and thus is more stable than 3D-min57. The phonon and band calculations were performed with the structure of 3D-min10, where the cell was redefined and reoptimized (see S5 in Supplemental Material [8] for the Cartesian coordinates). The phonon dispersion presented in S6 in Supplemental Material [8] shows that 3D-min10 is a local minimum structure. The band structure in Fig. 7 suggests that this structure is metallic. Furthermore, a

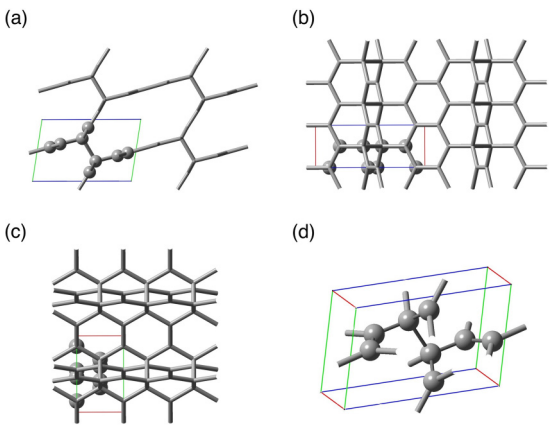

FIG. 6. Views along the *a* axis (a), *b* axis (b), and *c* axis (c), and the primitive cell (d) of 3D-min10. TVs are shown as red, green, and blue lines.

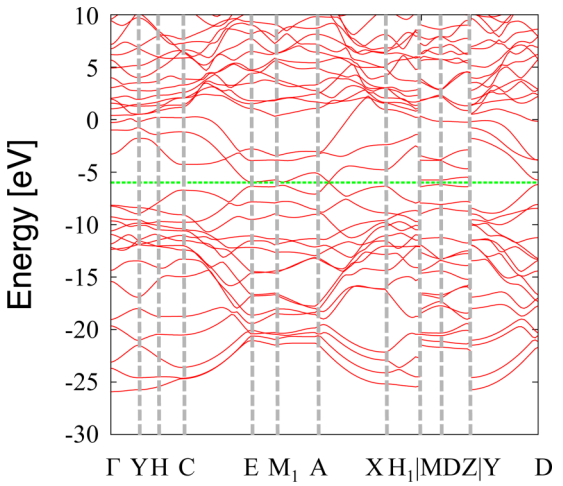

FIG. 7. Band structure of 3D-min10. The Fermi level is shown by a green line. The definitions of *k* points are described in Ref. [27] and S7 in Supplemental Material [8].

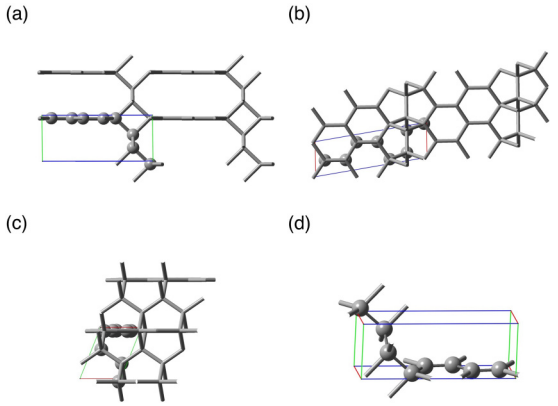

FIG. 8. Views along the a axis (a), b axis (b), and c axis (c), and the primitive cell (d) of 3D-min12. TVs are shown as red, green, and blue lines.

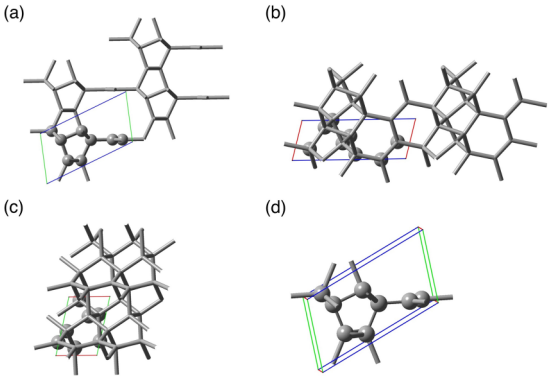

FIG. 10. Views along the a axis (a), b axis (b), and c axis (c), and the primitive cell (d) of 3D-min13. TVs are shown as red, green, and blue lines.

Dirac cone was found between the A and X points in the band structure of 3D-min10.

The second most stable structure among those newly found in this study, i.e., 3D-min12, is depicted in Fig. 8. The space group of this structure is $P1$. It includes eight carbon atoms in its primitive lattice. This structure is composed of sp^2 and sp^3 carbons and is similar to 3D-(4,4) carbon (3D-min23) [39,42]. Both of these structures have a large hollow, and the size and shape of the hollow are different for 3D-min12 and 3D-min23. The phonon and band calculations were conducted for 3D-min12 with the cell redefined and reoptimized (see S5 in Supplemental Material [8] for its Cartesian coordinates). Phonon dispersion indicates that 3D-min12 is a local minimum structure, as shown in S6 in the Supplemental Material [8]. The band structure in Fig. 9 shows that this structure is metallic.

The third most stable structure among those newly found in this study is 3D-min13. Its structure is depicted in Fig. 10 in various ways. The space group of this structure is $P1$. It includes eight carbon atoms in its primitive lattice. This structure is composed of sp^2 and sp^3 carbons and is similar to C_{CAS} [63]. Although both of these structure have five-membered rings and a large hollow, they are different from each other in their size of the hollow. The phonon and band calculations were conducted for 3D-min13 with the cell redefined and reoptimized (see S5 in Supplemental Material [8] for its Cartesian coordinates). Phonon dispersion indicates that 3D-min13 is a local minimum structure, as shown in S6 in the Supplemental Material [8]. The band structure in Fig. 11 shows that this structure also is metallic. Furthermore, two Dirac cones were found around the Y point and the L point in the band structure of 3D-min13.

Carbyne, shown in Fig. 12(a), was obtained as the 266th-lowest MIN (3D-min265) with a high relative energy of 112.3 kJ/mol atoms. Carbyne is a linear, pure-carbon chain described as a resonance structure of polyyne $(-C \equiv C-)_n$ and polycumulene $(=C=)_n$. Although short carbon chain molecules have been studied extensively [64–67], the production of very long chains composed of more than 6000 atoms has been achieved only recently in a double-walled CNT [68]. The present search found a structure, shown in Fig. 12(b), in which carbyne is sandwiched by graphene sheets (3D-min36). Intriguingly, the relative energy of the sandwiched structure of

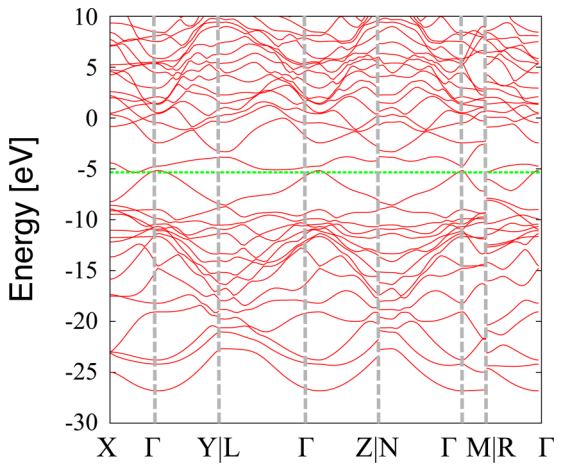

FIG. 9. Band structure of 3D-min12. The Fermi level is shown by a green line. The definitions of k points are described in Ref. [27] and S7 in Supplemental Material [8].

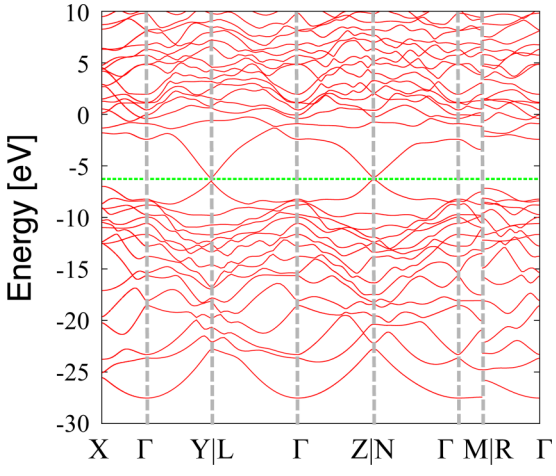

FIG. 11. Band structure of 3D-min13. The Fermi level is shown by a green line. The definitions of k points are described in Ref. [27] and S7 in Supplemental Material [8].

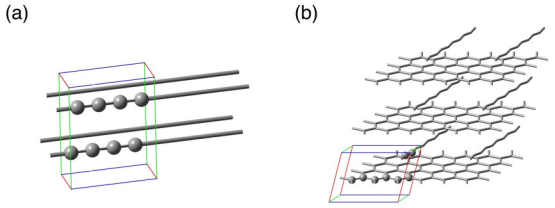

FIG. 12. The structures of (a) carbyne and (b) sandwiched carbyne. TVs are shown in red, green, and blue lines.

37.5 kJ/mol atoms is lower than the average energy of graphite and carbyne, which is 56.2 kJ/mol atoms. This suggests that carbyne is also stabilized by graphene sheets.

The present search missed a previously reported structure called 4H diamond [69] even though it can be written with the C_8 unit cell. In 4H diamond, structures of diamond and hexagonal diamond coexist, and its unit cell is highly elongated. The 4H diamond was missed because of the structural clustering, which was introduced in Sec. II D. The algorithm restricts the search to areas in which the shape of the unit cell is not far from cubic. As discussed in Sec. II D, this structure is expected to be found with the present algorithm if a larger unit cell is used. The other structures which were missed were K_4 [70–72] and D_{6h} prism-C_{12} [73]. This is because these structures have a much higher energy than 3D-min0. Hence, the present search, which is targeted to low-energy structures [16], was unable to find them. These structures can be found when larger P and M values are adopted, where P and M are the parameters of the stochastic search algorithm as defined in Sec. II A. We note that a K_4-like structure was predicted in the present search as 3D-min223, where its energy of 88.9 kJ/mol atoms is slightly higher than the K_4 83.3 kJ/mol atoms at the present computational level.

V. CONCLUSION

In this study, the AFIR method was combined with the PBCs. The AFIR method has been used extensively in the exploration of reaction pathways in molecular systems. The combined PBC/AFIR approach was applied to the carbon crystals described by the C_8 unit cell. The search automatically generated the previously reported low-lying structures. Furthermore, a lot of unreported structures were found. This suggests that the AFIR method is effective not only in molecular systems but also for the global exploration of low-lying crystal structures of a given atomic composition.

Among the many newly found structures, three low-lying structures were further studied. These three structures have a slightly higher energy than those predicted previously, such as Cco-C_8 (Z-carbon) and M-carbon. All three structures did not exhibit a band gap and were predicted to behave as a metal. Furthermore, Dirac cones were discovered in the band structures of two of these structures.

In addition, the present approach was extended for the exploration of two- or one-dimensional periodic structures. A search of two-dimensional periodic structures with C_8 unit cell gave many structures, such as two-dimensional sheets, composed of three-, four-, five-, six-, seven-, eight-, nine-, and/or ten-membered rings including graphene. Another search of the one-dimensional periodic structures with a C_8 unit cell found GNR, the thinnest CNT, carbyne, and so forth.

The present results suggest that this PBC/AFIR approach is promising in exploring low-lying periodic structures systematically. Furthermore, this approach, in principle, is applicable to any periodic system. Applications to systems including two or more elements and/or to molecular crystals will be interesting future avenues for research.

ACKNOWLEDGMENTS

M.T. is supported by the Ministry of Education, Culture, Sports, Science and Technology through the Program for Leading Graduate Schools (Hokkaido University "Ambitious Leader's Program"). This work was partly supported by a grant from Japan Science and Technology Agency with a Core Research for Evolutional Science and Technology (CREST) in the Area of "Establishment of Molecular Technology towards the Creation of New Functions" (Grant No. JPMJCR14L5) at Hokkaido University, Materials Research by Information Integration Initiative (MI^2I) project of the Support Program for Starting Up Innovation Hub from Japan Science and Technology Agency (JST), Japan.

[1] V. Georgakilas, J. A. Perman, J. Tucek, and R. Zboril, Chem. Rev. **115**, 4744 (2015).
[2] A. R. Oganov and C. W. Glass, J. Chem. Phys. **124**, 244704 (2006).
[3] Q. Li, Y. Ma, A. R. Oganov, H. Wang, H. Wang, Y. Xu, T. Cui, H.-K. Mao, and G. Zou, Phys. Rev. Lett. **102**, 175506 (2009).
[4] Z. Zhao, B. Xu, X.-F. Zhou, L.-M. Wang, B. Wen, J. He, Z. Liu, H.-T. Wang, and Y. Tian, Phys. Rev. Lett. **107**, 215502 (2011).
[5] M. Amsler, J. A. Flores-Livas, L. Lehtovaara, F. Balima, S. A. Ghasemi, D. Machon, S. Pailhès, A. Willand, D. Caliste, S. Botti, A. San Miguel, S. Goedecker, and M. A. L. Marques, Phys. Rev. Lett. **108**, 065501 (2012).
[6] Samara Carbon Allotrope Database (SACADA): see http://sacada.sctms.ru/ (accessed December 24, 2016).
[7] R. Hoffmann, A. A. Kabanov, A. A. Golov, and D. M. Proserpio, Angew. Chem., Int. Ed. **55**, 10962 (2016).
[8] See Supplemental Material at http://link.aps.org/supplemental/10.1103/PhysRevB.95.184110 for (S1) the full list of references on carbon crystal structures, (S2) the derivation of Eq. (1), (S3) initial structures, (S4) Cartesian coordinate of all obtained MINs, (S5) primitive lattice of 3D-min10, 3D-min12, and 3D-min13, (S6) phonon dispersion curve of 3D-min10, 3D-min12, and 3D-min13, and (S7) Symmetry k-points of 3D-min10, 3D-min12, and 3D-min13.
[9] D. J. Wales and H. A. Scheraga, Science **285**, 1368 (1999).
[10] K. Sanderson, Nature **450**, 771 (2007).
[11] A. R. Oganov, *Modern Methods of Crystal Structure Prediction* (John Wiley & Sons, Hoboken, NJ, 2011).
[12] C. J. Pickard and R. J. Needs, J. Phys.: Condens. Matter **23**, 053201 (2011).
[13] T. Gu, W. Luo, and H. Xiang, WIREs Comput. Mol. Sci. **7**, e1295 (2017).

[14] S. Maeda, K. Ohno, and K. Morokuma, Phys. Chem. Chem. Phys. **15**, 3683 (2013).
[15] S. Maeda, T. Taketsugu, and K. Morokuma, J. Comput. Chem. **35**, 166 (2014).
[16] S. Maeda, Y. Harabuchi, M. Takagi, T. Taketsugu, and K. Morokuma, Chem. Rec. **16**, 2232 (2016).
[17] W. M. C. Sameera, S. Maeda, and K. Morokuma, Acc. Chem. Res. **49**, 763 (2016).
[18] A. Banerjee, N. Adams, J. Simons, and R. Shepard, J. Phys. Chem. **89**, 52 (1985).
[19] D. Sánchez-Portal, P. Ordejón, E. Artacho, and J. M. Soler, Int. J. Quantum Chem. **65**, 453 (1997).
[20] J. M. Soler, E. Artacho, J. D. Gale, A. García, J. Junquera, P. Ordejón, and D. Sánchez-Portal, J. Phys.: Condens. Matter **14**, 2745 (2002).
[21] D. Sánchez-Portal, P. Ordejón, and E. Canadell, Struct. Bonding (Berlin, Ger.) **113**, 103 (2004).
[22] S. Grimme, J. Comput. Chem. **27**, 1787 (2006).
[23] GGA Pseudopotential Database: see http://departments.icmab.es/leem/siesta/Databases/Pseudopotentials/periodictable-gga-abinit.html (accessed May 3, 2016).
[24] A. Togo, computer code SPGLIB: see https://atztogo.github.io/spglib/ (accessed January 12, 2016).
[25] A. Togo, computer code PHONOPY: see https://atztogo.github.io/phonopy/ (accessed June 16, 2016).
[26] A. Togo, F. Oba, and I. Tanaka, Phys. Rev. B **78**, 134106 (2008).
[27] W. Setyawan and S. Curtarolo, Comput. Mater. Sci. **49**, 299 (2010).
[28] T. Bučko, J. Hafner, S. Lebègue, and J. G. Ángyán, J. Phys. Chem. A **114**, 11814 (2010).
[29] S. Bahmann, T. Weißbach, and J. Kortus, Phys. Status Solidi RRL **7**, 639 (2013).
[30] R. H. Baugbman and D. S. Galvgão, Chem. Phys. Lett. **211**, 110 (1993).
[31] P. A. Schultz, K. Leung, and E. B. Stechel, Phys. Rev. B **59**, 733 (1999).
[32] K. Umemoto, R. M. Wentzcovitch, S. Saito, and T. Miyake, Phys. Rev. Lett. **104**, 125504 (2010).
[33] H. S. Domingos, J. Phys.: Condens. Matter **16**, 9083 (2004).
[34] R. H. Baughman, A. Y. Liu, C. Cui, and P. J. Schields, Synth. Met. **86**, 2371 (1997).
[35] J. V. Badding and T. J. Scheidemantel, Solid State Commun. **122**, 473 (2002).
[36] R. T. Strong, C. J. Pickard, V. Milman, G. Thimm, and B. Winkler, Phys. Rev. B **70**, 045101 (2004).
[37] X.-F. Zhou, G.-R. Qian, X. Dong, L. Zhang, Y. Tian, and H.-T. Wang, Phys. Rev. B **82**, 134126 (2010).
[38] V. A. Greshnyakov and E. A. Belenkov, J. Exp. Theor. Phys. **113**, 86 (2011).
[39] Z. Zhao, B. Xu, L.-M. Wang, X.-F. Zhou, J. He, Z. Liu, H.-T. Wang, and Y. Tian, ACS Nano **5**, 7226 (2011).
[40] Q. Zhu, Q. Zeng, and A. R. Oganov, Phys. Rev. B **85**, 201407(R) (2012).
[41] X. Zhang, Y. Wang, J. Lv, C. Zhu, Q. Li, M. Zhang, Q. Li, and Y. Ma, J. Chem. Phys. **138**, 114101 (2013).
[42] M. Hu, J. He, Q. Wang, Q. Huang, D. Yu, Y. Tian, and B. Xu, J. Superhard Mater. **36**, 257 (2014).
[43] D. L. V. K. Prasad, N. M. Gerovac, M. J. Bucknum, and R. Hoffmann, J. Chem. Theor. Comput. **9**, 3855 (2013).
[44] M. J. Bucknum, E. A. Castro, and B. Wen, J. Math. Chem. **50**, 2281 (2012).
[45] C. Cheng, Z.-L. Lv, Y. Cheng, X.-R. Chen, and L.-C. Cai, Diamond Relat. Mater. **43**, 49 (2014).
[46] J. Fayos, J. Solid State Chem. **148**, 278 (1999).
[47] E. A. Belenkov and V. A. Greshnyakov, J. Exp. Theor. Phys. **119**, 101 (2014).
[48] R. Hoffmann, T. Hughbanks, and M. Kertisz, J. Am. Chem. Soc. **105**, 4831 (1983).
[49] G.-M. Rignanese and J.-C. Charlier, Phys. Rev. B **78**, 125415 (2008).
[50] R. H. Baughman and D. S. Galvao, Nature **365**, 735 (1993).
[51] X. Meng-Jiang, L. Bin-Hua, Y. Zheng-Tao, and C. Qi, Commun. Theor. Phys. **64**, 237 (2015).
[52] A. F. Wells, Acta Crystallogr. **7**, 535 (1954).
[53] A. T. Balaban, C. C. Rentia, and E. Ciupitu, Rev. Roum. Chim. **13**, 231 (1968).
[54] V. H. Crespi, L. X. Benedict, M. L. Cohen, and S. G. Louie, Phys. Rev. B **53**, R13303 (1996).
[55] M. Deza, P. W. Fowler, M. Shtogrin, and K. Vietze, J. Chem. Inf. Comput. Sci. **40**, 1325 (2000).
[56] B. R. Sharma, A. Manjanath, and A. K. Singh, Sci. Rep. **4**, 7164 (2014).
[57] H. Zhu, A. T. Balaban, D. J. Klein, and T. P. Živković, J. Chem. Phys. **101**, 5281 (1994).
[58] M. J. Bucknum and E. A. Castro, Solid State Sci. **10**, 1245 (2008).
[59] X.-Q. Wang, H.-D. Li, and J.-T. Wang, Phys. Chem. Chem. Phys. **14**, 11107 (2012).
[60] X.-L. Sheng, H.-J. Cui, F. Ye, Q.-B. Yan, Q.-R. Zheng, and G. Su, J. Appl. Phys. **112**, 074315 (2012).
[61] Z. Zhu and D. Tománek, Phys. Rev. Lett. **109**, 135501 (2012).
[62] F. J. Ribeiro, P. Tangney, S. G. Louie, and M. L. Cohen, Phys. Rev. B **72**, 214109 (2005).
[63] Z.-J. Wei, H.-Y. Zhao, J. Wang, and Y. Liu, J. Appl. Phys. **120**, 165101 (2016).
[64] R. I. Kaiser, Chem. Rev. **102**, 1309 (2002).
[65] F. Cataldo, *Polyynes: Synthesis, Properties, and Applications* (CRC Press/Taylor & Francis, Boca Raton, FL, 2005).
[66] C. S. Casari, M. Tommasini, R. R. Tykwinskic, and A. Milani, Nanoscale **8**, 4414 (2016).
[67] Y. Taguchi, H. Endo, T. Kodama, Y. Achiba, H. Shiromaru, T. Wakabayashi, B. Wales, and J. H. Sanderson, Carbon **115**, 169 (2017).
[68] L. Shi, P. Rohringer, K. Suenaga, Y. Niimi, J. Kotakoski, J. C. Meyer, H. Peterlik, M. Wanko, S. Cahangirov, A. Rubio, Z. J. Lapin, L. Novotny, P. Ayala, and T. Pichler, Nat. Mater. **15**, 634 (2016).
[69] K. E. Spear, A. W. Phelps, and W. B. White, J. Mater. Res. **5**, 2277 (1990).
[70] B. Winkler, C. J. Pickard, V. Milman, and G. Thimm, Chem. Phys. Lett. **337**, 36 (2001).
[71] T. Sunada, Not. Am. Math. Soc. **55**, 208 (2008).
[72] M. Itoh, M. Kotani, H. Naito, T. Sunada, Y. Kawazoe, and T. Adschiri, Phys. Rev. Lett. **102**, 055703 (2009).
[73] K. Ohno, H. Satoh, and T. Iwamoto, Chem. Phys. Lett. **633**, 120 (2015).